

Original Article

A radiologic diagnostic scoring model based on CT features for differentiating gastric schwannoma from gastric gastrointestinal stromal tumors

Jian-Xia Xu^{1*}, Jie-Ni Yu^{2*}, Xiao-Jie Wang², Yan-Xi Xiong³, Yuan-Fei Lu², Jia-Ping Zhou², Qiao-Mei Zhou², Xiao-Yan Yang², Dan Shi², Xiao-Shan Huang¹, Shu-Feng Fan^{1#}, Ri-Sheng Yu^{2#}

¹Department of Radiology, The Second Affiliated Hospital of Zhejiang Chinese Medical University, 318 Chao-Wang Road, Hangzhou 310005, Zhejiang Province, China; ²Department of Radiology, Second Affiliated Hospital, School of Medicine, Zhejiang University, 88 Jie-Fang Road, Hangzhou 310009, Zhejiang Province, China; ³Department of Radiology, Renmin Hospital, Hubei University of Medicine, Shiyuan 442000, Hubei Province, China. *Equal contributors and co-first authors. #Equal contributors.

Received August 18, 2021; Accepted December 27, 2021; Epub January 15, 2022; Published January 30, 2022

Abstract: We aimed to further explore the CT features of gastric schwannoma (GS), propose and validate a convenient diagnostic scoring system to distinguish GS from gastric gastrointestinal stromal tumors (GISTs) preoperatively. 170 patients with submucosal tumors pathologically confirmed (GS n=35; gastric GISTs n=135) from Hospital 1 were analyzed retrospectively as the training cohort, and 72 patients (GS=11; gastric GISTs=61) from Hospital 2 were enrolled as the validation cohort. We searched for significant CT imaging characteristics and constructed the scoring system via binary logistic regression and converted regression coefficients to weighted scores. The ROC curves, AUCs and calibration tests were carried out to evaluate the scoring models in both the training cohort and the validation cohort. For convenient assessment, the system was further divided into four score ranges and their diagnostic probability of GS was calculated respectively. Four CT imaging characteristics were ultimately enrolled in this scoring system, including transverse position (2 points), location (5 points), perilesional lymph nodes (6 points) and pattern of enhancement (2 points). The AUC of the scoring model in the training cohort were 0.873 (95% CI, 0.816-0.929) and the cutoff point was 6 points. In the validation cohort, the AUC was 0.898 (95% CI, 0.804-0.957) and the cutoff value was 5 points. Four score ranges were as follows: 0-3 points for very low probability of GS, 4-7 points for low probability; 8-9 points for middle probability; 10-15 points for very high probability. A convenient scoring model to preoperatively discriminate GS from gastric GISTs was finally proposed.

Keywords: Gastric schwannoma, gastrointestinal stromal tumors, scoring model, contrast-enhanced CT, gastric neoplasms

Introduction

Gastric schwannoma (GS) is a benign, rare, and generally slow-growing mesenchymal neoplasm which originates from the Schwann cell sheath, accounting for approximately only 8% of all stomach mesenchymal tumors [1-3]. GS is easily confused with a heterogeneous group of mesenchymal neoplasms such as gastric gastrointestinal stromal tumors (GISTs), the most common submucosal tumors of the stomach [4-8].

Though both GS and GISTs have no unique clinical characteristics and predominantly occur in the middle-aged persons, the prognosis for GS

and GISTs is very different [9, 10]. GS appears a low malignant potential and has a great prognosis after surgery [11, 12]. Whereas, 10-30% of GISTs have malignant behavior with recurrences and metastasis [13]. Accurate diagnosis is determined by pathology and immunohistochemistry which only can be performed on the surgical specimen, and strong positivity for S-100 protein has diagnostic significance for GS and the expression of KIT (CD117) is significant to differentiate GISTs from other mesenchymal tumors [14-17]. Therefore, it's important to distinguish GS from gastric GISTs preoperatively so as to provide advice to the clinical decision.

A radiologic scoring model for differentiating GS from gastric GISTs

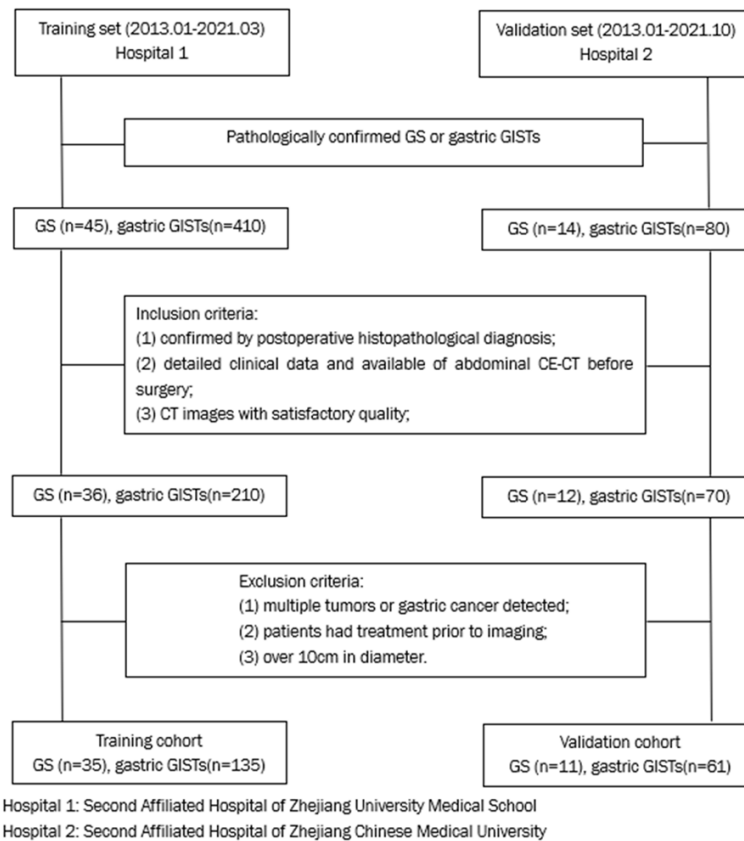


Figure 1. Flowchart of patient selection.

CT is viewed as an ideal imaging modality to discriminate GS from gastric GISTs before surgery for its wide utilization and non-invasiveness [9]. So far, some studies have reported the CT findings of GS [1, 9, 16, 18-21]. However, its CT imaging features have not been fully analyzed in these previous studies because of its rarity and most of these studies just gave descriptive analysis which couldn't obtain the result directly and easily.

Thus, this study aims to further explore the CT features of GS, and construct an easy scoring model for differentiating GS from gastric GISTs preoperatively.

Materials and methods

Patients

This retrospective study was waived informed consent from patients approved by the institutional review board of hospitals. The study population was obtained from two independent hospitals and 242 patients with GS or gastric

GISTs were ultimately enrolled. A total of 170 patients comprising of 35 with GS and 135 with gastric GISTs form the Second Affiliated Hospital of Zhejiang University Medical School (Hospital 1), diagnosed from January 2013 to March 2021, were assigned as the training cohort to determine the CT features for distinguishing GS from gastric GISTs and to further establish the scoring model. The validation cohort consisted of 11 GS patients and 61 gastric GISTs patients from the Second Affiliated Hospital of Zhejiang Chinese Medical University (Hospital 2), diagnosed from January 2013 to October 2021, to testify the performance of the scoring model. The inclusion criteria were as follows: (1) patients with GS or gastric GISTs were confirmed by postoperative histopathological diagnosis, including morphological and immunohistochemical assess-

ments of specimens; (2) patients had detailed clinical data and were available of abdominal CE-CT performed before surgery; (3) CT images with satisfactory quality contained non-enhanced phase, portal venous phase and equilibrium phase; (4) tumor size was large enough (≥ 0.5 cm in maximum diameter) to show clearly in the CT images. The exclusion criteria were as follows: (1) multiple tumors or gastric cancer was detected; (2) patients had treatment prior to imaging; (3) tumor size was larger than 10 cm in maximum diameter (**Figure 1**).

CT imaging acquisition

Every patient was told to fast for at least 6 hours before the abdominal CE-CT examinations. Ten minutes prior to scanning, every patient was injected 10 mg anisodamine intramuscularly and drank 800-1000 ml water orally. Abdominal CE-CT examinations in Hospital 1 were performed on one multidetector-row CT (SOMATOM Definition Flash; Siemens Healthcare, Germany) and in Hospital 2 were per-

A radiologic scoring model for differentiating GS from gastric GISTs

Table 1. Clinical characteristics of GS and gastric GISTs in the training cohort: univariate analysis

Clinical characteristics	GS (n=35)	Gastric GISTs (n=135)	P*
Age	55.97±10.13	60.16±10.48	0.035
Gender			0.122
Male	12 (34.3%)	66 (48.9%)	
Female	23 (65.7%)	69 (51.1%)	
Abdominal discomfort			0.384
No	15 (42.86%)	69 (51.1%)	
Yes	20 (57.14%)	66 (48.9%)	

*P values ≤0.05 shown as bold and italics indicated a statistically significant difference between groups.

Table 2. Clinical characteristics of GS and gastric GISTs in the validation cohort: univariate analysis

Clinical characteristics	GS (n=11)	GIST (n=61)	P*
Age	61.00±8.75	59.72±9.01	0.665
Gender			1.000
Male	5 (45.45%)	26 (42.62%)	
Female	6 (54.55%)	35 (57.38%)	
Abdominal discomfort			0.095
No	7 (63.64%)	21 (34.43%)	
Yes	4 (36.36%)	40 (65.57%)	

*P values ≤0.05 written in bold and italics indicates a statistically significant difference between two groups.

formed on two CT scanners: a Lightspeed VCT (GE Healthcare; Chicago; IL) and on Optima 540 (GE Healthcare). Patients were imaged in a supine position scanned from the diaphragmatic top to the pubic symphysis. The CT parameters were as follows: tube voltage 120 kVp, tube current 200 mA, detector configuration 128×0.6 mm, slice thickness 5 mm, slice interval 5 mm, pitch 0.6 mm. The contrast agents were Ultravist (Bayer Schering Pharma; Berlin; Germany) in Hospital 1 and Optiray (Liebel-Flarsheim Canada Inc.; Kirkland; Quebec; Canada), respectively. A total of 100 ml of nonionic iodinated contrast medium was injected via a pump injector at 5 ml/sec into an antecubital vein. The portal venous phase and the equilibrium phase were performed at 50-60 s and 100-110 s after the injection of contrast agent, respectively. The sagittal and coronal images were reconstructed with a 1.5-mm section thickness and a 1.5-mm interval after scanning.

Imaging interpretation

All images were interpreted by consensus of two experienced abdominal radiologists (with 15 and over 30 years of experience, respectively) independently and retrospectively, who were blinded to the histopathological outcome.

The CT features included the long diameter/the short diameter (LD/SD) ratio of the tumors, transverse position (anterior wall, posterior wall, greater curvature or lesser curvature), location (cardia, fundus, body or antrum), growth pattern (intraluminal, extraluminal or mixed), contour (round, ovoid or irregular), surface ulceration (presence or absence), margin (well-defined or ill-defined), calcification (presence or absence), adjacent organs invasion (presence or absence), necrosis (presence or absence), intratumoral and peritumoral enlarged vessels (presence or absence), perilesional enlarged lymph nodes (presence or absence), pattern of enhancement (homogeneous or heterogeneous) and degree of enhancement (mild, moderate or strong). Besides, attenuation values in the non-enhanced phase, portal venous phase and equilibrium phase were measured in the largest dimension of the tumor. After that, difference value 1 (the portal venous phase values minus the non-enhanced phase values), difference value 2 (the equilibrium phase values minus the non-enhanced phase values) and difference value 3 (the equilibrium phase values minus the portal venous phase values) were calculated. Enhancement characteristics and enlarged vessels were observed in the equilibrium phase.

The long diameters and short diameters were measured on the center slices of images in three different orientations. Transverse position was the location of the lesion on the cross section usually observed in the coronal and sagittal orientations. Surface ulcerations were defined as focal tissue detected in the surface of the tumor. Necrosis was considered as present when there was non-enhancing tissue with a CT attenuation value of 0-20 HU in the tumor. The perigastric lymph nodes were viewed as present when their shortest diameters were

A radiologic scoring model for differentiating GS from gastric GISTs

Table 3. CT features comparison among GS and gastric GISTs in the training cohort: univariate analysis

CT Features	GS (n=35)	Gastric GISTs (n=135)	P*
LD/SD ratio	1.26±0.17	1.24±0.21	0.638
Transverse position			<0.001
Anterior wall	6 (17.14%) ^{a,b}	20 (14.81%) ^{a,b}	
Posterior wall	3 (8.57%) ^b	43 (31.85%) ^b	
Lesser curvature	8 (22.85%) ^b	47 (34.81%) ^b	
Greater curvature	18 (51.43%) ^a	25 (18.52%) ^a	
Location			<0.001
Cardia	0 (0.00%) ^{a,b}	8 (5.93%) ^{a,b}	
Fundus	3 (8.57%) ^b	58 (42.96%) ^b	
Body	26 (74.29%) ^a	53 (39.26%) ^a	
Antrum	6 (17.14%) ^a	16 (11.85%) ^a	
Growth pattern			0.020
Intraluminal	7 (20.00%)	62 (45.93%)	
Extraluminal	17 (48.57%)	43 (31.85%)	
Mixed	11 (31.43%)	30 (22.22%)	
Contour			0.499
Round	14 (40.00%)	67 (49.63%)	
Ovoid	15 (42.86%)	44 (32.59%)	
Irregular	6 (17.14%)	24 (17.78%)	
Surface ulceration			0.082
Absent	32 (91.43%)	106 (78.52%)	
Present	3 (8.57%)	29 (21.48%)	
Margin			0.320
Well-defined	31 (88.57%)	110 (81.48%)	
Ill-defined	4 (11.43%)	25 (18.82%)	
Calcification			0.529
Absent	33 (94.29%)	121 (81.48%)	
Present	2 (5.71%)	14 (10.37%)	
Adjacent organs invasion			0.005
Absent	35 (100.00%)	109 (80.74%)	
Present	0 (0.00%)	26 (19.26%)	
Necrosis			0.707
Absent	24 (68.57%)	88 (65.19%)	
Present	11 (31.43%)	47 (34.81%)	
Intratumoral enlarged vessels			1.000
Absent	30 (85.71%)	117 (86.67%)	
Present	5 (14.29%)	18 (13.33%)	
Peritumoral enlarged vessels			0.301
Absent	22 (62.86%)	97 (71.85%)	
Present	13 (37.14%)	38 (28.15%)	
Perilesional lymph nodes			<0.001
Absent	27 (77.14%)	133 (98.52%)	
Present	8 (22.86%)	2 (1.48%)	
Pattern of enhancement			0.031
Homogeneous	26 (74.29%)	73 (54.07%)	
heterogeneous	9 (25.71%)	62 (45.93%)	

larger than 5 mm [9]. Patterns of enhancement were defined as follows: it was considered as homogeneous enhancement if the difference value between the most strongly and weakly enhanced section of the lesions was less than 10 HU, or else, viewed as heterogeneous enhancement. The degree of enhancement was quantitatively evaluated by the difference value between the post-enhanced CT value (the larger of either portal venous phase or the equilibrium phase) and the non-enhanced CT value of the same portion of the lesion. If the difference value was <20 HU, it was considered as mild enhancement pattern; 20-40 HU was regarded as moderate enhancement pattern, and >40 HU as strong enhancement pattern. CT attenuation values of the lesions were measured with a 20 mm² circular region-of-interest (ROI) encompassing as much of the most strongly enhanced section of the lesion as possible. Meanwhile, avoid calcification, hemorrhage, necrosis, cystic degeneration, blood vessels in tumor and adjacent structures. The quantitative data was tested at least three times for each lesion and then the calculated mean values were used to analyze.

Statistical analysis

Numerical data was shown as the mean ± standard deviation (M±SD) and categorical data was shown as frequency (percentages). Continuous variables were compared using the Student t test and categorical variables were compared with the help of the chi-square or Fisher's exact test between two groups in univari-

A radiologic scoring model for differentiating GS from gastric GISTs

Degree of enhancement			0.133
Mild	4 (11.43%)	27 (20.00%)	
Moderate	14 (40.00%)	66 (48.89%)	
Strong	17 (48.57%)	42 (31.11%)	
Value of non-enhanced phase	35.74±5.20	34.79±6.63	0.436
Value of portal venous phase	63.20±15.85	56.32±14.48	0.015
Value of equilibrium phase	76.67±19.52	66.82±17.55	0.004
Difference value 1	27.46±14.73	21.53±14.59	0.034
Difference value 2	40.94±18.84	32.02±17.14	0.008
Difference value 3	13.48±10.87	10.50±12.72	0.206

a, b: the same letter markers indicated no statistical difference. **P* values ≤0.05 shown as bold and italics indicated a statistically significant difference between groups.

in the training cohort were summarized and compared in **Table 1**. The present study revealed no significant difference with regard to gender and abdominal discomfort, but had a difference in mean age between GS group (55.97±10.13 years) and gastric GISTs group (60.16±10.48 years) (*P*=0.035) in the training cohort. The cutoff point for age was 62.5 based on the ROC curve analysis.

ate analysis. Each Variable presented significant statistically in univariate analysis was obtained into collinearity diagnostics and further obtained in a binary logistic regression model with a backward stepwise approach to confirm independent predictors of GS and construct the ultimate predictive model. To establish a simple-to-calculate scoring system, we divided every regression coefficient by one-half of the smallest coefficient and rounded to the nearest integer to convert regression coefficient to weighted scores [22]. The overall scores which were produced through summing up the individual scores corresponding to the predictors ranged from 0 to 15. Calibration was evaluated by the Hosmer-Lemeshow goodness-of-fit test and the receiver operating characteristic (ROC) curve and the area under curve (AUC) was used to assess the discriminatory power of models. Delong nonparametric method was performed to compare the ROCs of various models (Delong and others 1988). A two-side *P* value ≤0.05 was viewed significant statistically.

All data was performed by SPSS version 26.0 software (IBM SPSS Statistics Version 26.0, IBM Corp.), except comparison of ROCs using MedCalc software, version 19.8 (MedCalc Software bvba).

Results

Clinical characteristics

A total of 170 patients, comprising 35 with GS and 135 with gastric GISTs were enrolled as the training cohort. The clinical characteristics

There were 72 patients were studied in the validation cohort, which contained 11 with GS and 61 with gastric GISTs. **Table 2** showed there were no significant difference in the age, gender or abdominal discomfort in the validation cohort according to the univariate analysis (*P*>0.05).

Predictors of preoperative diagnosis model of GS

The comparison of CT imaging features in the training cohort was shown in **Table 3** that demonstrated important difference in the transverse position (*P*<0.001), location (*P*<0.001), growth pattern (*P*=0.020), adjacent organs invasion (*P*=0.005), perilesional lymph nodes (*P*<0.001), pattern of enhancement (*P*=0.031), value of portal venous phase (*P*=0.015), value of equilibrium phase (*P*=0.004), difference value 1 (*P*=0.034) and difference value 2 (*P*=0.008). The relativity of the four predictors mentioned above for discriminating GS from gastric GISTs in the training cohort was demonstrated by a Venn diagram (**Figure 2**). The same comparison and analysis were performed in the validation cohort. All relevant predictors in the training cohort maintained statistical difference in the validation cohort apart from adjacent organs invasion. LD/SD ratio (*P*=0.044) also showed significant difference in the training cohort (**Table 4**).

Establishment of a preoperative predictive model

Predictors associated with the CT features of GS in univariate analysis in the training cohort

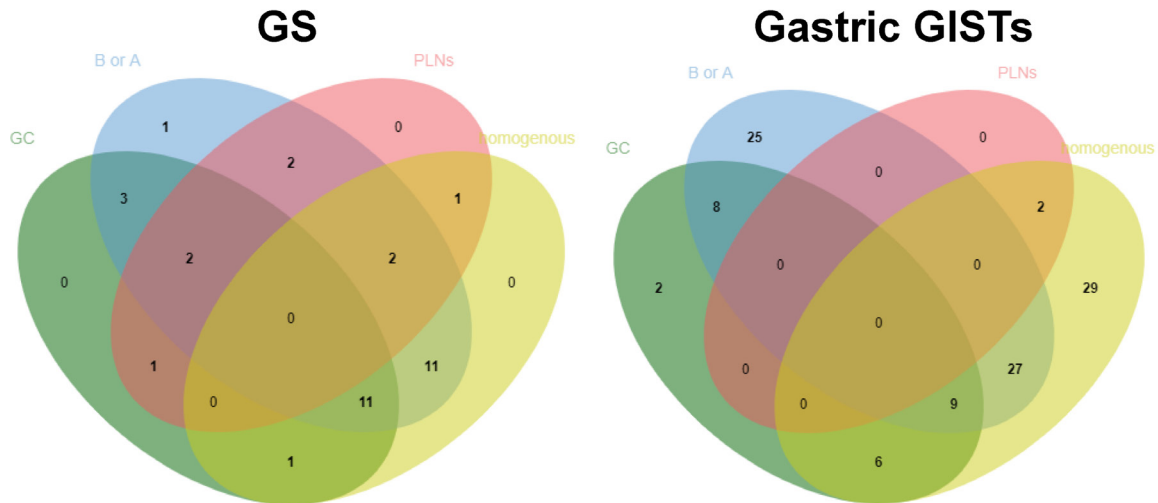


Figure 2. The correlation of the four predictors for discriminating GS from gastric GISTs in the training cohort was demonstrated by a Venn diagram (<http://jvenn.toulouse.inra.fr/app/example.html>).

Table 4. CT features comparison among GS and gastric GIST in the validation cohort: univariate analysis

CT features	GS (n=11)	GIST (n=61)	P*
LD/SD ratio	1.16±0.09	1.24±0.20	0.044
Transverse position			0.001
Anterior wall	3 (27.27%)	13 (21.31%)	
Posterior wall	0 (0.00%)	22 (36.07%)	
Lesser curvature	1 (9.09%)	17 (27.87%)	
Greater curvature	7 (63.64%)	9 (14.75%)	
Location			0.022
Cardia	0 (0.00%)	5 (8.20%)	
Fundus	1 (9.09%)	28 (45.90%)	
Body	7 (63.64%)	23 (37.70%)	
Antrum	3 (27.27%)	5 (8.20%)	
Growth pattern			<0.001
Intraluminal	0 (0.00%)	30 (49.18%)	
Extraluminal	6 (54.55%)	25 (40.98%)	
Mixed	5 (45.45%)	6 (9.84%)	
Contour			0.290
Round	7 (63.64%)	26 (42.62%)	
Ovoid	3 (27.27%)	16 (26.23%)	
Irregular	1 (9.09%)	19 (31.15%)	
Surface ulceration			1.000
Absent	10 (90.91%)	53 (86.89%)	
Present	1 (9.09%)	8 (13.11%)	
Margin			0.192
Well-defined	11 (100.00%)	49 (80.33%)	
Ill-defined	0 (0.00%)	12 (19.67%)	
Calcification			0.337

were obtained into collinearity diagnostics and were proved no significant multicollinearity. Then multivariate binary logistic regression showed four independent predictors for GS diagnosis distinguishing from gastric GISTs, which included transverse position (OR, 4.8; 95% CI, 1.8-12.7; P=0.001), location (OR, 31.9; 95% CI, 3.8-264.3; P=0.001), perilesional lymph nodes (OR, 127.3; 95% CI, 11.1-1464.5; P<0.001) and pattern of enhancement (OR, 0.2; 95% CI, 0.1-0.7; P=0.008), as presented in **Table 5**, which were adopted to establish the scoring model. The results of Hosmer-Lemeshow goodness-of-fit test ($\chi^2=2.457$; P=0.783) indicated great calibration of this predictive model. The AUC value of this model showed well (0.872, 95% CI, 0.816-0.929, P<0.001).

Establishment of a scoring model

To provide a quantitative method to predict GS (**Figure 3**) from gastric GISTs (**Figure 4**), we

A radiologic scoring model for differentiating GS from gastric GISTs

Absent	11 (100.00%)	52 (85.25%)	
Present	0 (0.00%)	9 (14.75%)	
Adjacent organs invasion			0.679
Absent	10 (90.91%)	48 (78.69%)	
Present	1 (9.09%)	13 (21.31%)	
Necrosis			0.055
Absent	11 (100.00%)	43 (70.49%)	
Present	0 (0.00%)	18 (29.51%)	
Intratumoral enlarged vessels			0.585
Absent	11 (100.00%)	54 (88.52%)	
Present	0 (0.00%)	7 (11.48%)	
Peritumoral enlarged vessels			0.438
Absent	8 (72.73%)	50 (81.97%)	
Present	3 (27.27%)	11 (18.03%)	
Perigastric lymph nodes			0.003
Absent	8 (72.73%)	61 (100.00%)	
Present	3 (27.27%)	0 (0.00%)	
Pattern of enhancement			0.047
Homogeneous	9 (81.82%)	28 (45.90%)	
heterogeneous	2 (18.18%)	33 (54.10%)	
Degree of enhancement			0.129
Mild	0 (0.00%)	14 (22.95%)	
Moderate	6 (54.55%)	33 (54.10%)	
Strong	5 (45.45%)	14 (22.95%)	
Value of non-enhanced phase	35.78±4.21	33.06±6.79	0.204
Value of portal venous phase	74.04±17.59	54.39±14.98	<0.001
Value of equilibrium phase	79.40±16.80	63.12±15.87	0.003
Difference value 1	38.26±16.17	21.33±13.67	<0.001
Difference value 2	43.62±16.26	30.06±13.48	0.004
Difference value 3	5.37±9.30	8.73±13.17	0.421

*P values ≤0.05 written in bold and italics indicates a statistically significant difference between two groups.

their AUCs. Hosmer-Lemeshow goodness-of-fit test of the scoring model in the training cohort showed good calibration (P=0.491), and the AUC value was 0.873 (95% CI, 0.816-0.929; P<0.001). The comparison of ROCs between predictive and scoring model in the training cohort presented no statistically significant difference (P=0.9385>0.05) testified by DeLong test, demonstrating the scoring model made great use of the information of the predictive model (**Figure 5**). In the training cohort, the median score was 5, with extremes of 0 and 13. If the cutoff point of score was set at 6 points, the specificity of this scoring model was 65.9% and the sensitivity was 94.3%.

Score ranges exploration

For the convenient usage of this scoring model in daily work, scores were further divided into four ranges: 0-3 points; 4-7 points; 8-9 points; 10-15 points. The positive predictive rates rose in the training cohort as shown in **Table 6** when level increased.

adopted a scoring model based on binary logistic regression analysis in the training cohort. We attached weighted score to each independent predictor, which as follows: transverse position on the greater curvature, 2 points; location on the body or antrum, 5 points; perilesional lymph nodes present, 6 points; homogeneous enhancement, 2 points, as shown in **Table 5**. The total scores ranged from 0 to 15 after adding up the individual scores related to the predictors.

Predictive performance of model in the training cohort

To validate and compare the diagnostic power of predictive and scoring model, we performed ROC comparison analysis and calculated

External validation of the established scoring model

In the validation cohort, Hosmer-Lemeshow test of the models presented good calibration (P>0.05). The AUCs of the predictive model and scoring model were 0.881 (95% CI, 0.783-0.945) and 0.898 (95% CI, 0.804-0.957), respectively. The comparison of ROCs between two models in the validation cohort showed no statistical difference (P=0.3794>0.05) testified by DeLong test (**Figure 6**). The median score was 5 with extremes of 0 and 15. The specificity was 81.97% and the sensitivity was 81.82% when the cutoff value was 5 points. The positive predictive rates of GS in the validation cohort were shown in **Table 7**.

A radiologic scoring model for differentiating GS from gastric GISTs

Table 5. Binary logistic regression analysis for GS diagnosis and the weighed score of independent predictors

Variables	B	P	OR	95% CI	Weighted Score
Transverse position (greater curvature)	1.572	0.001	4.8	1.8-12.7	2
Location (body or antrum)	3.461	0.001	31.9	3.8-264.3	5
Perilesional lymph nodes (present)	4.847	<0.001	127.3	11.1-1464.5	6
Pattern of enhancement (homogeneous)	-1.523	0.008	0.2	0.1-0.7	2
Constant	-4.570	<0.001	0.01		

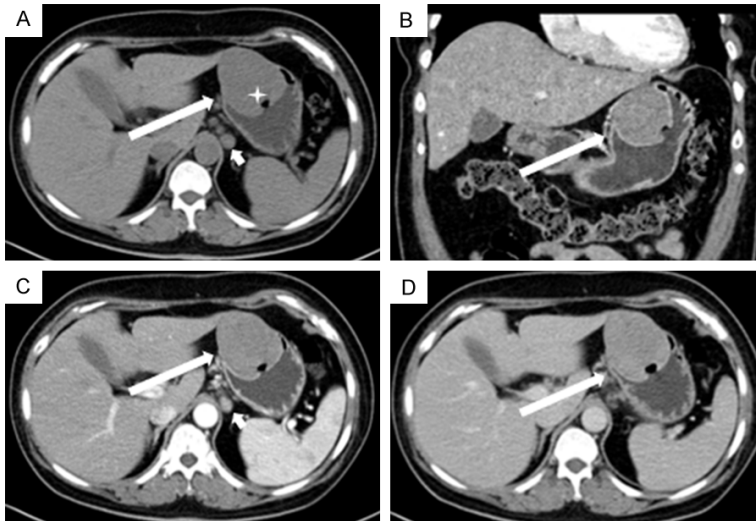


Figure 3. GS in a 49-year-old woman detected by accident. A. Axial unenhanced CT scan depicts an ovoid and well-defined mass (arrow) with homogeneous attenuation. There is an enlarged lymph node (arrowhead) nearby and surface ulceration (star) in the tumor. B. Coronal orientation CT scan shows the neoplasm (arrow) grows in the lesser curvature of the body of the stomach. C and D. Axial contrast-enhanced CT scan (portal venous phase and equilibrium phase, respectively) shows homogeneous enhanced mass (arrow). This patient scored 13 points.

Discussion

GS and gastric GISTs are both submucosal tumors of the stomach and GS is often misdiagnosed as gastric GISTs [7]. Considering that GS has a good prognosis after surgery whereas GISTs shows a malignant potential, distinguishing them has important clinical implications. The definitive diagnoses of GS and gastric GISTs require immunohistochemical studies which are invasive and postoperative [4]. In order to obtain more information before surgery so as to guide the clinical treatment, CT is an ideal choice and we aim to identify CT features capable of distinguishing these neoplasms.

The maximum diameters of the tumors analyzed in this study were no larger than 10 cm. There were two reasons why we made such design to select patients. For one thing, there was only one person with a GS which was over 10 cm in diameter in our cohort, which means that GS rarely grows very large as a slow-growing neoplasm. For the other thing, according to the standard of risk stratification proposed by Joensuu [23], GISTs with diameters over 10 cm are viewed as high-risk GISTs which are easier to distinguish from GS.

In the training cohort, the clinical data of GS and gastric GISTs was similar and without specificity except age. Though both GS and gastric GISTs predominantly occur in the mid-

dle age, GS was more often found in patients younger than 62.5 years in the training cohort. This finding is consistent with previous studies [1, 9]. However, all clinical characteristics of GS and gastric GISTs had no significant difference in the validation cohort and the different result of age between the training cohort and the validation cohort may result from the small sample size.

There were four variables viewed as the independent predictors of the GS differentiating from gastric GISTs in the training cohort. Compared with previous studies [18, 24], the result of the presence of regional lymphadenopathy was similar to ours, and the OR was 127.3

A radiologic scoring model for differentiating GS from gastric GISTs

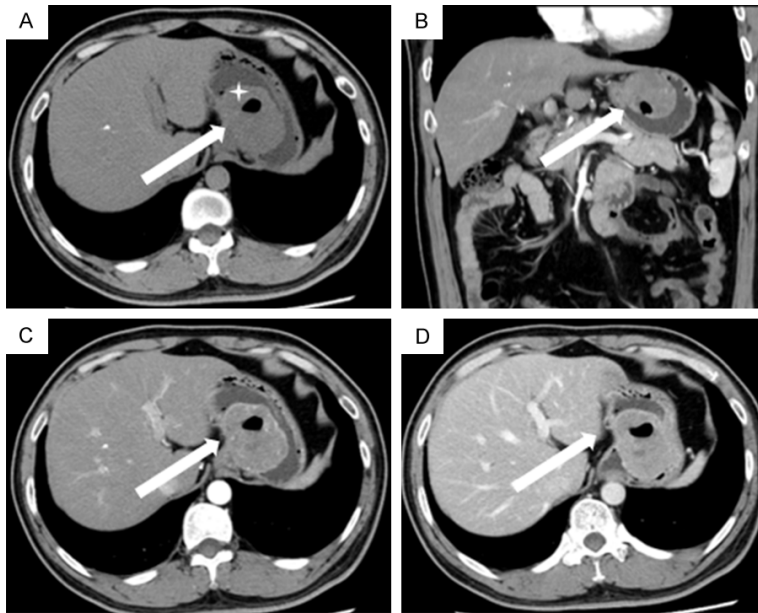


Figure 4. Gastric GISTs in 39-year-old man with hematemesis. A. Axial unenhanced CT scan presents an ovoid and well-defined tumor (arrow) with heterogeneous attenuation and surface ulceration (star). B. Coronal CT scan indicates the mass (arrow) grows in the lesser curvature of the fundus of the stomach. C and D. Axial contrast-enhanced CT scan (portal venous phase and equilibrium phase, respectively) shows heterogeneously enhanced mass (arrow) with necrosis. There is no obvious perilesional lymph node. This patient scored 0 point.

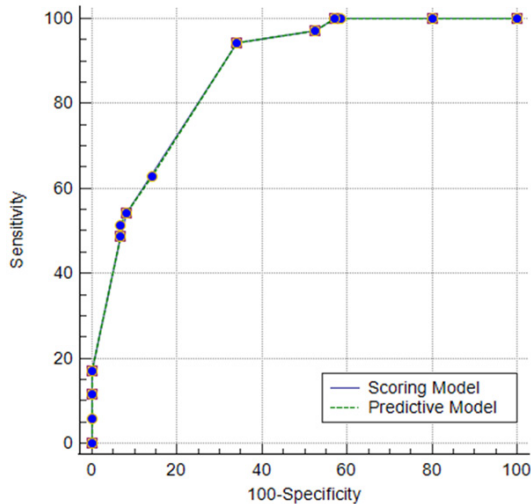


Figure 5. ROC curves of predictive and scoring model in GS diagnosis in the training cohort.

(95% CI 11.1-1464.5) that weighted the highest score, indicating perilesional lymph nodes present is the most significant characteristic of GS distinguishing from gastric GISTs. Choi, et al. [18] presumed that these perigastric lymph

nodes present reactive inflammation. In this study, enlarged lymph nodes around GS were all benign hyperplasia of lymph nodes without evidence of malignancy.

In the training cohort, location and transverse position were other two independent variables of this scoring model with weighted score secondary to the presence of lymphadenopathy (OR 31.9, 95% CI 3.8-264.3; OR 4.8, 95% CI 1.8-12.7, respectively). In the univariate analysis, we divided the stomach into four parts respectively to locate the lesion according to the anatomy, which were as follows: cardia, fundus, body or antrum in the location and anterior wall, posterior wall, greater curvature or lesser curvature in the transverse position. We found that GS tended to grow in the large curve of the gastric body

whereas gastric GISTs were often seen in the posterior wall or small curve of the fundus of the stomach, which was consistent with the previous study [1, 19]. There was no statistical difference between cardia and fundus, which was same between body and antrum. As a consequence, in the establishment of preoperative predictive model, location was presented as either cardia and fundus or body and antrum. Transverse position was presented as whether on the greater curvature or not for the same reason.

The pattern of enhancement demonstrated statistically significant difference in the two groups in the training cohort and this was the last predictor of our scoring model (OR 0.2, 95% CI 0.1-0.7). GS presented homogeneous enhancement in 74.29% of cases in the training cohort, demonstrating that GS, as a slow-growing mesenchymal neoplasm, often lacks of degenerative transformations, such as hemorrhage and necrosis [21]. However, with a varying malignancy potential, gastric GISTs are often consisted of a heterogeneous mass due to necrosis or hemorrhage [9, 13, 17, 25, 26].

A radiologic scoring model for differentiating GS from gastric GISTs

Table 6. Patients with GS in four score ranges in the training cohort

Score groups	Numbers of patients with Gastric Schwannoma	Total number	Diagnostic probability of GS
0-3 points	0	58	0%
4-7 points	16	82	About 19.5%
8-9 points	13	24	About 54%
10-15 points	6	6	100%

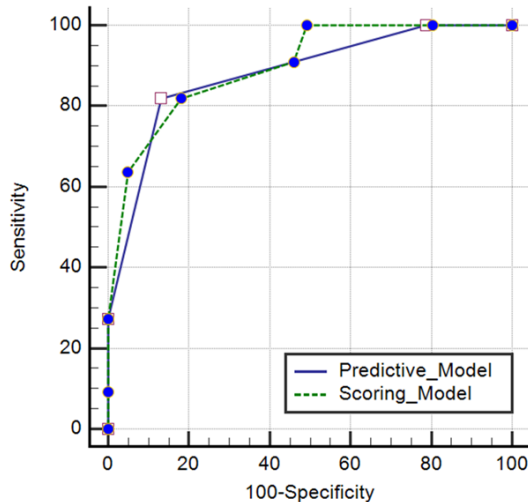


Figure 6. ROC curves of predictive and scoring model in GS diagnosis in the validation cohort.

We noticed that GS tended to show extraluminal or mixed growth pattern whereas gastric GISTs were more likely to present as endophytic tumors in both the training cohort and the validation cohort. Although growth pattern wasn't included in our logistic regression model, both Choi, et al. [18] and Wang, et al. [19] confirmed that there was statistical difference between two groups, reminding us to pay attention to it and perform further exploration in the future.

The final scoring system established in our study could successfully differentiated GS from gastric GISTs through observing four CT imaging features, including perilesional lymph nodes present, location on the body or antrum, transverse position on the greater curvature, and homogeneous enhancement. The scores ranged from 0 to 15 and were further divided into four groups according to the distribution, then diagnostic probability of GS for each group in the training cohort was calculated respec-

tively (**Table 6**). None of 58 patients was GS if the score ≤ 3 . When the score ranged from 4 to 7, 16 out of 82 (about 19.5%) patients had GS. Patients with GS accounted about 54% (13/24) when score was 8 or 9. If score was over 9, the diagnostic probability of GS was 100% (6/6).

To assess the generalizability of the scoring model, an external validation cohort was substituted into both scoring model and score range to verify the discrimination ability. The AUC (0.898; 95% CI, 0.804-0.957) reflected good discrimination ability of the scoring model in the validation cohort and the score range showed satisfactory predictive performance (**Table 7**).

The weighted scores of each predictor were in a range of 2 to 6 based on binary logistic regression analysis. If no more than one of these four CT features could be found, scores must less than 7, which indicated there was much more chance to be diagnosed as gastric GISTs instead of GS. In contrast, if patients got a score over 9, tumors must grow in the gastric body or antrum with regional lymphadenopathy or grow in the greater curvature of the stomach with homogeneous enhancement and perilesional enlarged lymph nodes. In this case, we could diagnose GS rather than gastric GISTs with confidence. By the way, though our model showed 100% probability of GS when patients scored over 9, the real situation may not be consistent with the model considering the bias caused by our small sample size. Nonetheless, when a patient got a score of 8 or 9, the probability of GS or gastric GISTs was almost half-to-half, which was difficult to make a final decision (**Table 8**). As a consequence, a prospective study containing a larger number of patients with gastric submucosal neoplasms is urgently needed to verify and further improve this scoring model.

There were also some limitations in our study. Firstly, this was a retrospective study with inherent potential for bias. Secondly, to our knowledge, though our sample was the largest, the size of our study population was still small, especially for GS. Considering that plentiful fac-

A radiologic scoring model for differentiating GS from gastric GISTs

Table 7. Patients with GS in four score ranges in the validation cohort

Score groups	Numbers of patients with Gastric Schwannoma	Total number	Diagnostic probability of GS
0-3 points	0	31	0%
4-7 points	4	31	About 12.9%
8-9 points	4	7	About 57.1%
10-15 points	3	3	100%

Table 8. The scoring model for preoperative prediction of GS from gastric GISTs

Predictive factors	Score	Probability-Total Score
Transverse position		
Except for greater curvature	0	
Greater curvature (GC)	2	
Location		
Cardia or fundus	0	Very low probability: 0-3 points
Body or antrum (B or A)	5	Low probability: 4-7 points
Perilesional lymph nodes (PLNs)		Middle probability: 8-9 points
Absence	0	Very high probability: 10-15 points
Present	6	
Pattern of enhancement		
Heterogeneous	0	
Homogeneous	2	

tors were compared between groups, the stability of the model may be affected and the false-positive rates may increase. Maybe that's the cause why our logistic regression model didn't contain growth pattern as a predictor in the training cohort. Thirdly, we excluded lesions larger than 10 cm in diameter, which may induce selection bias.

In conclusion, we proposed and validated a new scoring model for radiologic diagnosis of GS discriminating from gastric GISTs with CT, which included the presence of perilesional lymph nodes, location, transverse position and pattern of enhancement. It's convenient and relatively reliable for radiologists, especially for the beginners. Prospective studies with larger sample sizes are warranted to testify and improve the model in the future.

Acknowledgements

This study was supported by grants from the Medical Science and Technology Project of the Health Department of Zhejiang Province of China (No. 2021KY839 and No. 2019334245).

Disclosure of conflict of interest

None.

Abbreviations

GS, gastric schwannoma; GISTs, gastrointestinal stromal tumors; CE-CT, contrast-enhanced computed tomography; LD, long diameter; SD, short diameter; HU, Hounsfield Units; ROI, region-of-interest; ROC, receiver operating characteristic; AUC, area under the curve; OR, odds ratio; CI, confidence interval; GC, greater curvature; B or A, body or antrum; PLNs, perilesional lymph nodes.

Address correspondence to:

Ri-Sheng Yu, Department of Radiology, Second Affiliated Hospital, School of Medicine, Zhejiang University, 88 Jie-

Fang Road, Hangzhou 310009, Zhejiang Province, China. Tel: +86-0571-87783925; E-mail: rishengyu@zju.edu.cn; Shu-Feng Fan, Department of Radiology, The Second Affiliated Hospital of Zhejiang Chinese Medical University, 318 Chao-Wang Road, Hangzhou 310005, Zhejiang Province, China. Tel: +86-135-8815-1376; E-mail: shufengfan@163.com

References

- [1] Wang J, Zhang W, Zhou X, Xu J and Hu HJ. Simple analysis of the computed tomography features of gastric schwannoma. *Can Assoc Radiol J* 2019; 70: 246-253.
- [2] Pu C and Zhang K. Gastric schwannoma: a case report and literature review. *J Int Med Res* 2020; 48: 300060520957828.
- [3] Yoon HY, Kim CB, Lee YH and Kim HG. Gastric schwannoma. *Yonsei Med J* 2008; 49: 1052-1054.
- [4] Shah AS, Rathi PM, Somani VS and Mulani AM. Gastric schwannoma: a benign tumor often misdiagnosed as gastrointestinal stromal tumor. *Clin Pract* 2015; 5: 775.
- [5] Tao K, Chang W, Zhao E, Deng R, Gao J, Cai K, Wang G and Zhang P. Clinicopathologic features of gastric schwannoma: 8-year experi-

A radiologic scoring model for differentiating GS from gastric GISTs

- ence at a single institution in China. *Medicine (Baltimore)* 2015; 94: e1970.
- [6] Li J, Ye Y, Wang J, Zhang B, Qin S, Shi Y, He Y, Liang X, Liu X, Zhou Y, Wu X, Zhang X, Wang M, Gao Z, Lin T, Cao H and Shen L; Chinese Society of Clinical Oncology CSCO Expert Committee on Gastrointestinal Stromal Tumor. Chinese consensus guidelines for diagnosis and management of gastrointestinal stromal tumor. *Chin J Cancer Res* 2017; 29: 281-293.
- [7] Nishida T, Blay JY, Hirota S, Kitagawa Y and Kang YK. The standard diagnosis, treatment, and follow-up of gastrointestinal stromal tumors based on guidelines. *Gastric Cancer* 2016; 19: 3-14.
- [8] Miettinen M, Sobin LH and Lasota J. Gastrointestinal stromal tumors of the stomach: a clinicopathologic, immunohistochemical, and molecular genetic study of 1765 cases with long-term follow-up. *Am J Surg Pathol* 2005; 29: 52-68.
- [9] Li R, Gan H, Ni S, Fu Y, Zhu H and Peng W. Differentiation of gastric schwannoma from gastric gastrointestinal stromal tumor with dual-phase contrast-enhanced computed tomography. *J Comput Assist Tomogr* 2019; 43: 741-746.
- [10] Nishida T, Goto O, Raut CP and Yahagi N. Diagnostic and treatment strategy for small gastrointestinal stromal tumors. *Cancer* 2016; 122: 3110-3118.
- [11] Wu X, Li B, Zheng C and He X. Clinical characteristics and surgical management of gastrointestinal schwannomas. *Biomed Res Int* 2020; 2020: 9606807.
- [12] Li B, Liang T, Wei L, Ma M, Huang Y, Xu H, Shi X and Qin C. Endoscopic interventional treatment for gastric schwannoma: a single-center experience. *Int J Clin Exp Pathol* 2014; 7: 6616-6625.
- [13] von Mehren M and Joensuu H. Gastrointestinal stromal tumors. *J Clin Oncol* 2018; 36: 136-143.
- [14] Tao LP, Huang EJ, Li P and Lu YY. Schwannoma of stomach: a clinicopathologic study of 12 cases. *Int J Clin Exp Pathol* 2018; 11: 1679-1683.
- [15] Mekras A, Krenn V, Perrakis A, Croner RS, Kalles V, Atamer C, Grützmänn R and Vassos N. Gastrointestinal schwannomas: a rare but important differential diagnosis of mesenchymal tumors of gastrointestinal tract. *BMC Surg* 2018; 18: 47.
- [16] Hong HS, Ha HK, Won HJ, Byun JH, Shin YM, Kim AY, Kim PN, Lee MG, Lee GH and Kim MJ. Gastric schwannomas: radiological features with endoscopic and pathological correlation. *Clin Radiol* 2008; 63: 536-542.
- [17] Levy AD, Remotti HE, Thompson WM, Sobin LH and Miettinen M. Gastrointestinal stromal tumors: radiologic features with pathologic correlation. *Radiographics* 2003; 23: 283-304, 456; quiz 532.
- [18] Choi JW, Choi D, Kim KM, Sohn TS, Lee JH, Kim HJ and Lee SJ. Small submucosal tumors of the stomach: differentiation of gastric schwannoma from gastrointestinal stromal tumor with CT. *Korean J Radiol* 2012; 13: 425-433.
- [19] Wang W, Cao K, Han Y, Zhu X, Ding J and Peng W. Computed tomographic characteristics of gastric schwannoma. *J Int Med Res* 2019; 47: 1975-1986.
- [20] Ji JS, Lu CY, Mao WB, Wang ZF and Xu M. Gastric schwannoma: CT findings and clinicopathologic correlation. *Abdom Imaging* 2015; 40: 1164-1169.
- [21] Levy AD, Quiles AM, Miettinen M and Sobin LH. Gastrointestinal schwannomas: CT features with clinicopathologic correlation. *AJR Am J Roentgenol* 2005; 184: 797-802.
- [22] Ben Ayed H, Koubaa M, Hammami F, Marrakchi C, Rekik K, Ben Jemaa T, Maaloul I, Yaich S, Damak J and Ben Jemaa M. Performance of an easy and simple new scoring model in predicting multidrug-resistant enterobacteriaceae in community-acquired urinary tract infections. *Open Forum Infect Dis* 2019; 6: ofz103.
- [23] Joensuu H. Risk stratification of patients diagnosed with gastrointestinal stromal tumor. *Hum Pathol* 2008; 39: 1411-1419.
- [24] Choi YR, Kim SH, Kim SA, Shin CI, Kim HJ, Kim SH, Han JK and Choi BI. Differentiation of large (≥ 5 cm) gastrointestinal stromal tumors from benign subepithelial tumors in the stomach: radiologists' performance using CT. *Eur J Radiol* 2014; 83: 250-260.
- [25] Liu M, Liu L and Jin E. Gastric sub-epithelial tumors: identification of gastrointestinal stromal tumors using CT with a practical scoring method. *Gastric Cancer* 2019; 22: 769-777.
- [26] El-Menyar A, Mekhodathil A and Al-Thani H. Diagnosis and management of gastrointestinal stromal tumors: an up-to-date literature review. *J Cancer Res Ther* 2017; 13: 889-900.